IEEE Access
Multidisciplinary ⋮ Rapid Review ⋮ Open Access Journal

Received 29 October 2024, accepted 20 November 2024, date of publication 25 November 2024,
date of current version 16 December 2024.

Digital Object Identifier 10.1109/ACCESS.2024.3505605

RESEARCH ARTICLE

VEIN-RING: A Wearable Dorsal Finger Vein Biometric Scanner

TEODORS EGLITIS, (Student Member, IEEE), EMANUELE MAIORANA, (Senior Member, IEEE), AND PATRIZIO CAMPISI, (Fellow, IEEE)

Department of Industrial, Electronic, and Mechanical Engineering, Roma Tre University, 00146 Rome, Italy

Corresponding author: Emanuele Maiorana (emanuele.maiorana@uniroma3.it)

This work was supported in part by the European Union under the Italian National Recovery and Resilience Plan (NRRP) of NextGenerationEU, partnership on "Telecommunications of the Future" (PE00000001 - program "RESTART" - Spoke 4 - Cascade Call Project "EXperience and Privacy for Extended RealiTy" - "EXPERT").

ABSTRACT Vascular biometrics is gaining popularity in academic research, industrial systems, and public acceptance mainly because vein patterns are not exposed and thus offer more security against presentation attacks than traditional biometric traits. Likewise, wearable systems have begun to enter our lives more widely, primarily due to their convenience and the possibility of employing them in the framework of two-factor authentication mechanisms. This paper presents a new wearable vascular biometrics technology: a dorsal finger vein biometric scanner that can be worn as a ring and used for continuous user recognition. This device evolves a project developed for finger vein biometrics, and it is fully open-source. We provide all the necessary materials to replicate the device: the circuit schematics, the printed circuit board Gerber, the components list, the models for the 3D-printed case, and the software required for device control and database management. We have collected and made available a database of 30 subject/180 class dorsal finger vein images, with preliminary recognition results with HTER = 14.6%, using basic preprocessing and the Maximum Curvature/Miura Match pipeline, indicating potential for further research.

INDEX TERMS Biometrics, wearable biometrics, vein biometrics, open-source.

I. INTRODUCTION

Over the past few decades, there has been a surge in the demand for affordable and easily deployable biometric recognition systems for a wide range of applications, from access control to consumer devices, from border control to surveillance, among other examples. Popular biometric modalities currently used in commercial devices to automatically identify individuals include facial recognition, fingerprint analysis, iris scanning, and voice recognition.

However, conventional biometric systems rely on exposed traits, making them vulnerable to presentation attacks. These attacks involve an attempt to deceive a biometric system by presenting spoofed samples during data capture to gain unauthorized access. Among the most innovative biometric approaches, hand vein pattern recognition is gaining traction in academic and industrial circles, primarily because of its inherent advantages. Vein patterns in the fingers, palm, back of the hand, and wrist are less susceptible to presentation attacks since they are not exposed to the public. Furthermore, these systems can be designed to use contactless methods for data capture, enhancing user convenience and ease of use.

In the late 1980s, vascular patterns were introduced as a potential biometric identifier [1]. This concept leverages the ability of near-infrared (NIR) light to penetrate human skin, and the fact that blood hemoglobin absorbs NIR light. More specifically, visible light is unsuitable for capturing the vein structures beneath the skin because skin and subcutaneous tissues have high light-scattering coefficients. However, when higher wavelengths in the NIR range are used, the scattering coefficients in human tissues are significantly reduced, allowing light to penetrate the skin. In the NIR spectrum, the degree of light penetration is influenced by the light relative absorption properties of water (H_2O) and hemoglobin in the blood. This latter is classified into oxyhemoglobin (HbO_2), which is saturated with oxygen, and deoxyhemoglobin (Hb), which is not. Typically, NIR light-emitting diodes (LEDs) with wavelengths in the $[810, 950]$ nm range are used for

The associate editor coordinating the review of this manuscript and approving it for publication was Zahid Akhtar.

illumination to exploit both the property of NIR light to penetrate the human skin and the absorption property of the blood hemoglobin of NIR light [2], with most systems relying on the 850 nm wavelength. Specifically, the high absorption coefficients of HbO_2 and Hb at wavelengths below 600 nm give blood its red color, since other colors are absorbed in greater proportions. In the NIR range, the absorption coefficient of hemoglobin is lower than that of the visible range, but still significantly higher than that of water. To capture vascular patterns, a camera with NIR sensitivity has to operate in conjunction with LEDs in the same NIR wavelength range. In such imaging system, veins appear as darker lines against the surrounding areas. This principle applies to various parts of the body.

This paper presents an open-source,[1] wearable device designed to acquire a small portion of the dorsal finger vein pattern, which we refer to as ring finger vein. We provide the necessary information for replicating the device and the software to control data collection, enabling other researchers to conduct independent acquisition studies. The goal is to collaboratively build a large and diverse dataset, which could potentially reduce bias issues [3] by harnessing the collective efforts of different teams worldwide. Our contributions can be summarized as follows:

- we design an open-source, low-cost, ring-sized wearable device for capturing dorsal finger vein patterns. We offer the core schematics, the printed circuit board (PCB) Gerber and drill files, 3D models for the 3D-printed case, and the ESP32 C project;
- we provide device control and data collection software, which manages calibration, illumination, digital gain, image capture, and database administration, all in Python;
- we offer an assembly manual and a data collection guide to help users build and operate the device;
- we include a plug-in for integrating with the `bob.bio.vein` platform [4], allowing for baseline result reproduction;
- we test the presented device on a database collected from 30 subjects, with six fingers per subject, and five samples for each class. This dataset is publicly available, and we also report baseline recognition performance to demonstrate the effectiveness of our ring finger vein acquisition device.

The paper is organized as follows. An overview of the current research on hand vein biometric recognition and on the related commercially-available products is briefly provided in Section II. In Section III, the proposed data collection device hardware is described in detail. The device software modules are described in Section V. Section VI describes data acquisition and management. The collected database and the preliminary data analysis performed on it are described in Sections VII and VIII, respectively. Future directions and conclusions are finally drawn in Section IX.

[1] https://gitlab.com/biomedia4n6-public/open_ring_vein_device

II. STATE OF THE ART

As mentioned in Section I, all the acquisition devices employed in hand vein biometric recognition system require a NIR illumination module and an image sensor capable of obtaining data in the NIR spectrum, while they can be differentiated depending on the relative position of the camera and the illuminator, and on the specific part of the hand that has to be acquired. In more detail, vein acquisition devices can work according to two distinct modalities: reflective or transmittive. In case the former modality is used, the illumination module is located on the same side as the imaging sensor, concerning the acquired part of the hand, so that the portion of emitted light reflected by the body is captured by the sensor. When resorting to the transmittive modality, the interested vein patterns are between the NIR source and the image sensor, so that the camera captures the portion of emitted light that passes through the considered body part. Reflective illumination is employed in several commercial devices developed for vein-based biometric recognition, such as the Hitachi touchless finger VeinID reader[2] or the Fujitsu PalmSecure device.[3] The use of reflective illumination in commercial devices, where the illuminator and the acquisition camera are placed on the same side of the device, guarantees better usability and helps to keep the device size small, although it requires to design dedicated hardware components and architectures. Conversely, the vast majority of academic research on hand-vein recognition relied on devices exploiting transmissive illumination due to the associated capability of acquiring better-quality images, given the possibility of confining the employed NIR light to a region of interest and excluding most external interferences.

As for the parts of the hands that have been taken into account to conduct vein-based biometric recognition, such list include finger vein [5], palm vein [6], wrist vein [7], and hand-dorsal vein [8]. Most of the research has focused on finger and palm vein patterns, mainly due to the possibility of achieving better recognition results when exploiting these traits, and the interest of the companies mentioned above. It is worth noting that the vein patterns commonly acquired when dealing with fingers are those on the palmar side. Several public datasets are available for this specific modality, with most academic studies conducted on samples extracted, among the others, from the Peking University (PKU) database [9], the Shandong University Machine Learning and Applications - Homologous Multimodal Traits (SDUMLA-HMT) database [10], the Idiap Research Institute Finger Vein Database (VERA) [11], and the University of Twente Finger Vascular Pattern (UTFVP) database [12]. Vein patterns from the finger dorsal side have been instead considered only in a limited number of studies, due to the availability of only a few datasets with such characteristics.

[2] https://www.hitachi.com/products/it/veinid/

[3] https://www.fujitsu.com/global/services/security/offerings/biometrics/palmsecure/

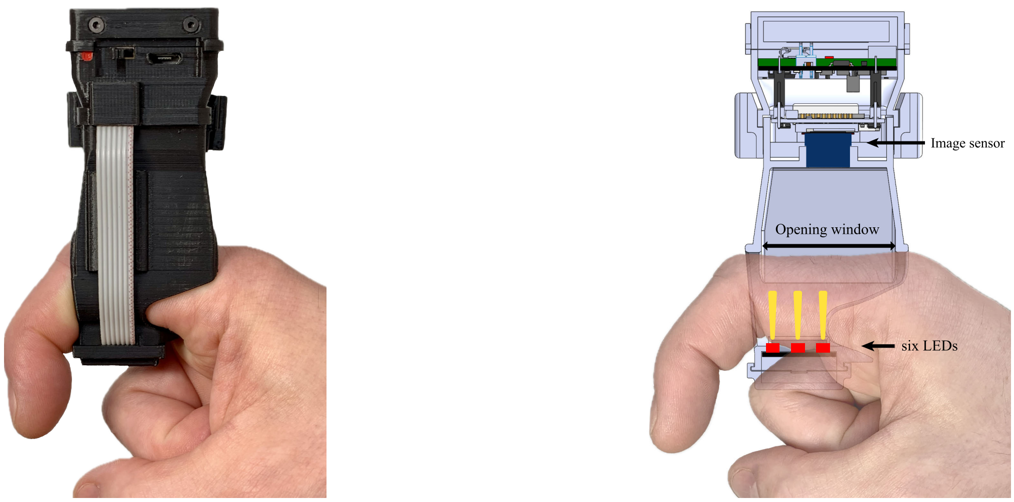

FIGURE 1. Ring device worn on right hand, index finger. (a): picture of the device; (b): artistic representation of the operation principle, i.e, light penetrates the skin while an image sensor captures the vascular patterns through the opening window.

Notably, images of dorsal finger vein patterns have been collected only in the Protect Multimodal database (PMMDB) [13], the PLUSVein-FV3 database [14], and the PLUSVein Finger rotation (FR) database [15], which contains images collected from 361 perspectives at different orientations for each finger. The vein patterns here considered are those in the dorsal side of the fingers, thus making our evaluation one of the few ones investigating the discriminative properties of this trait.

The need to investigate dorsal finger vein patterns derives from design constraints we considered when developing the presented acquisition device, whose most notable characteristics are being wearable and easily transportable. Given the growing diffusion of smart devices that can be worn on fingers, such as the already available Oura ring[4] or the Samsung Galaxy Ring, which will be released in the near future,[5] we have developed a device that can collect images of finger-vein patterns while being worn. As it will be detailed in Section III, to give a user the possibility to move the hands and the fingers as freely as possible, the most significant prominent part of the device, i.e., the one housing the acquisition camera, was designed to be on the dorsal side of the hand, with only the illumination part left in the palmar side of the fingers, thus leaving the possibility to close a hand without significant hindrance.

The development of wearable devices that capture images of hand vein patterns has been attempted so far only in a few studies. The first attempt toward this aim was performed by the Biowatch [16], a device designed to collect wrist vein patterns by placing sensors on a watch wristband. In this case, samples were acquired when putting the watch on the wrist, keeping the sensors at a proper distance from the vein patterns. Since data collection has to be performed before wearing the device, continuous recognition cannot be accomplished. A similar design was considered for the prototype presented by [17], where Diffuse Optical Tomography (DOT) was exploited to build a relatively compact device able to collect wrist vein images. For more exhaustive reviews on the state of the art on vein biometrics, which is out of the scope of this paper, interested readers can refer to [18] and [19].

The open-source project upon which this work also relies has been presented in [20], where a device collecting images of the whole finger palmar side was proposed. This paper addresses a topic that has so far been little explored and is potentially very interesting for application developments related to the possibility of performing vein-based biometric recognition using wearable devices by exploiting and evaluating the vein patterns in the dorsal side of fingers.

III. THE RING VEIN SYSTEM

This paper presents a novel device that leverages our open-source project in [20], where finger vein patterns have been acquired using a standalone, modular, and open-source device. Instead, in this work, we focus on a novel finger vein modality, where only a tiny dorsal portion of the finger is interested in the acquisition procedure to simulate a ''smart ring''. The prototype we present here is intended as a proof of concept of a wearable device to acquire subcutaneous vein patterns. This makes the technology functional and adaptable to current consumer trends, enabling biometrics to be paired with fitness tracking, health monitoring, and other wearable functionalities when using, for example, the already

[4] https://ouraring.com/

[5] https://www.samsungmobilepress.com/media-assets/galaxy-ring

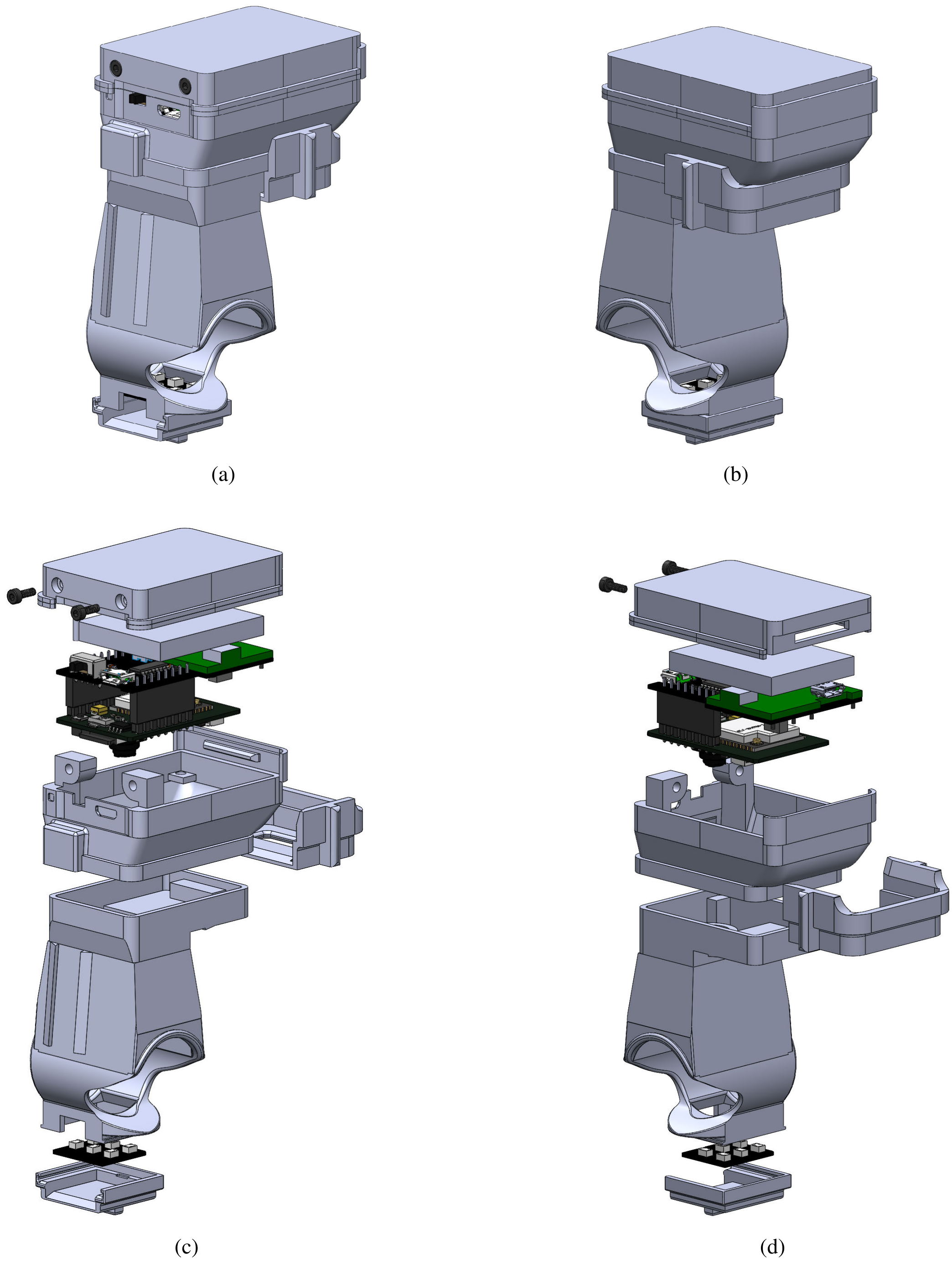

FIGURE 2. Device 3-D rendering from different perspectives. (a) and (b): assembled views; (c) and (d): exploded views.

commercialized smart rings[6] capable of monitoring sleep, health, and more in general wellness.

Specifically, the developed device has the following characteristics:

- *modular*: it is composed of an imaging module that has been adequately designed to be used to acquire different vascular parts of the hand;
- *standalone*: it is a relatively small size device, wearable, and with wireless capabilities to be connected with the PC hosting the collected data;
- *open-source*: the project is open-source in both hardware and software, and the device can be built using widely available and low-cost components.

Figure 1(a) shows a picture of the device as it is worn, with the camera module on top and the illumination module on

[6]e.g. https://gloringstore.com

TABLE 1. **Illumination board's part list.**

Name	Designator	Footprint
SFH 4651-UV – 860nm OSRAM LED	D0, D1, D2, D3, D4, D5	SFH 4651-UV (custom)
Connector 1.27mm (0.05inch) pitch, male, 2x4 SMD	J1	Connector 1.27mm 2x4 SMD
7X1 pin 2.54mm female header	J2	7X1-2.54mm

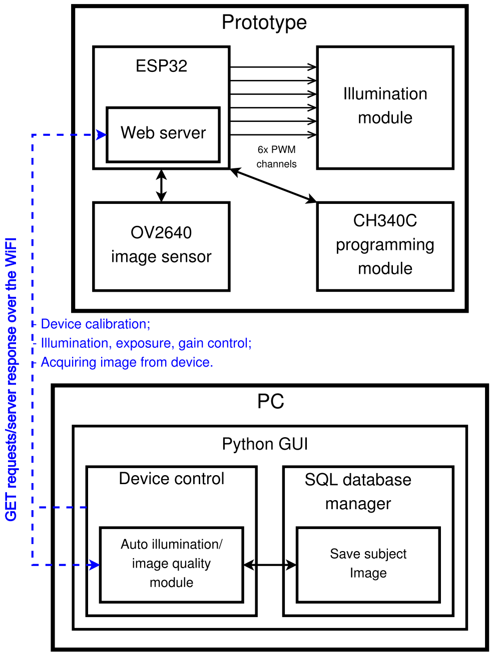

FIGURE 3. **Diagram representing device and its control.**

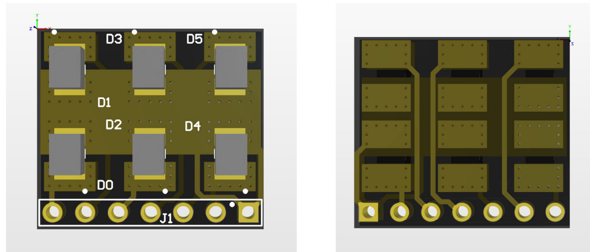

(a) (b)

FIGURE 4. **Rendering of the illumination board. (a): top; (b): bottom.**

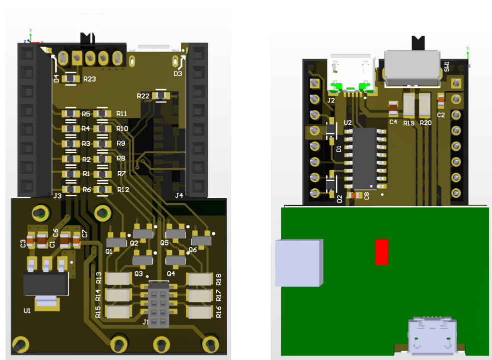

(a) (b)

FIGURE 5. **Rendering of main board's layers. (a): top; (b): bottom.**

the bottom. This choice is justified by the actual integration level of the device and specifically by the camera dimension, which suggests the device use as in Figure 1, thus optimizing user comfort and long-term wearability. The device works in transmissive modality. Figure 1(b) shows a graphical representation of a section of the device. At the bottom of the device, six NIR SMD LEDs provide the needed illumination. The finger is inserted in proper support, as shown in the picture, and the camera module finally acquires the image. Some renderings of the 3-D device are shown in Figure 2 under different angles.

The system, whose functional scheme is in Figure 3, comprises an acquisition device, i.e., the camera module and the LED illumination module, the main board to power and control the device, and the enclosure, described in Section IV. The software module to control device illumination and data acquisition is detailed in Section V. The dataset manager, described in Section VI, handles the acquired data.

IV. THE RING VEIN DEVICE: THE HARDWARE

In this section, the device hardware modules are detailed.

A. THE CAMERA MODULE

We have chosen to base our development system on ESP32 family microcontrollers [21], since they have gained considerable popularity in recent years. The chosen development board, the ESP32-CAM AI-Thinker (ESP32-CAM) [22], is among the most compact development boards with camera support. The ESP32-CAM comes equipped with an ESP32-S system-on-a-chip (SOC) microcontroller featuring a dual-core, 32-bit, 240 MHz CPU, integrated WiFi, and security functionalities, including IEEE 802.11 support, secure boot, flash encryption, and cryptographic hardware acceleration. Additionally, the ESP32-CAM includes an external 8MB PSRAM and is compatible with the OmniVision OV2640 image sensor. It features a TF card slot and two LEDs, one of which serves as a camera flash. Without a TF card, 5 GPIOs are available for use, and this number can be expanded to 6 by eliminating the built-in flash. Introduced in 2005, the OV2640 component is the first fully integrated Type 1/4-inch 2 MP, 1600 × 1200 (UXGA) resolution image sensor. It is obtainable in a Compact Camera Module with an M7 format lens. The sensor lacks a NIR filter and offers various lens options for purchase. Our experimentation found that the optimal lens for the application possesses

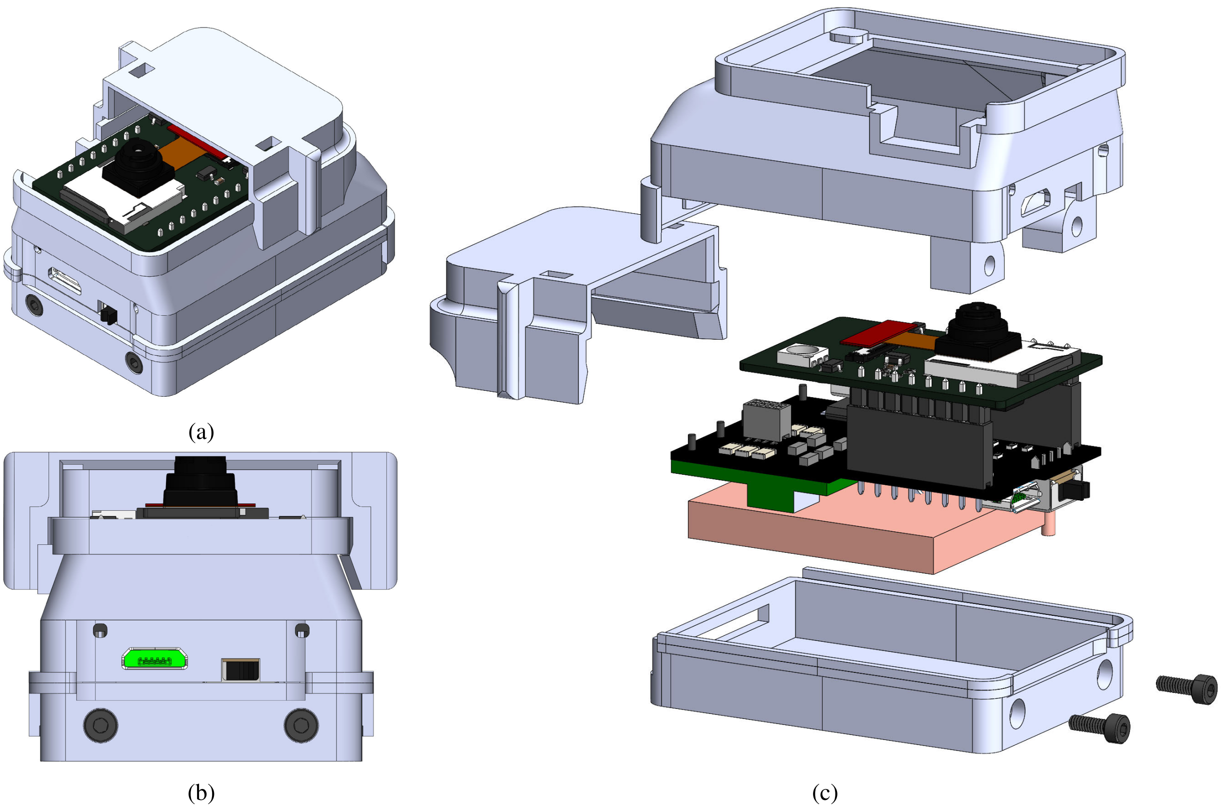

FIGURE 6. **Acquisition module. (a): 3D view; (b): side view; (c): exploded view.**

FIGURE 7. **Ring finger holders: sizes 16 to 26 mm.**

a Field of View of 160°, an f/2.4 aperture, and lacks an NIR filter.

We have designed two PCBs: the main board and LED illumination board, as described in Sections IV-C and IV-B, respectively to ensure easy replication of the device.

B. THE LED ILLUMINATION MODULE

The illumination module is located at the bottom of the device, as shown in Figures 2(c) and 2(d), and has dimensions 15.7 × 17.5 mm. The board layout is shown in Figures 4 and the components are listed in Table 1. Specifically, we are

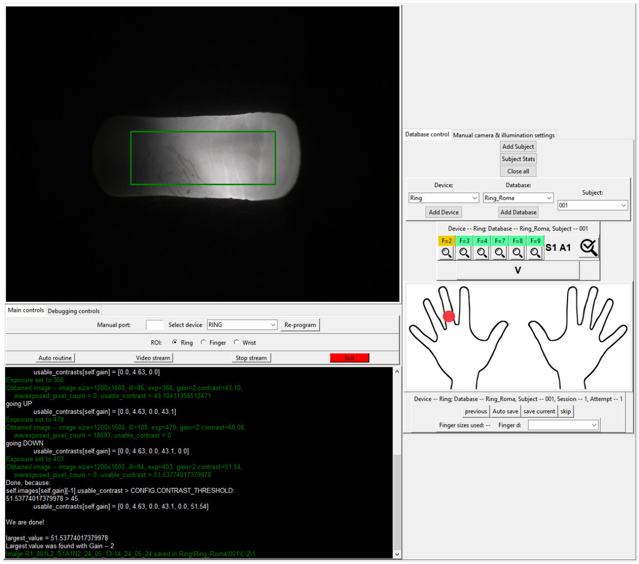

FIGURE 8. **GUI: device controls (leftside) and the database controls (rightside).**

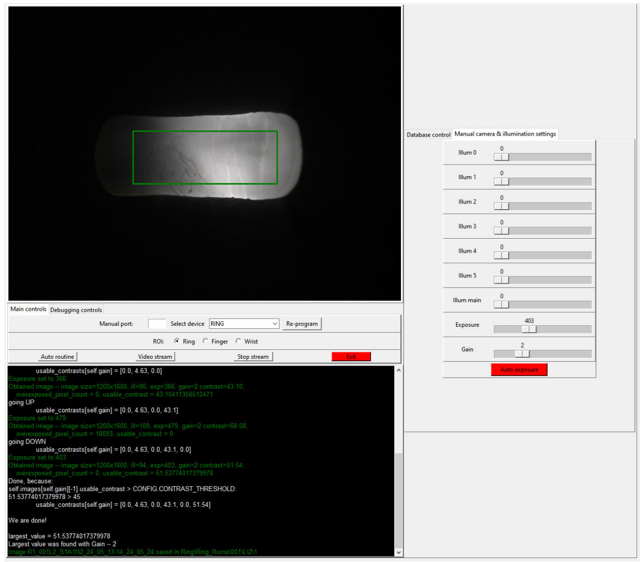

FIGURE 9. **GUI: device controls (leftside) and the illumination controls (rightside).**

using 6 OSRAM 850 nm LEDs with a maximal $I_F = 70$ mA and a narrow illumination half-angle of 10°, with the possibility to set different duty cycles and thus the brightness for each of the LEDs.

C. THE MAIN BOARD

The main board (MB) houses all necessary electronic parts to power and run the ESP32-CAM. It can be assembled in two configurations: battery-powered and powered through the USB connector. It has the following functions:

- housing of the optional battery charging module;
- power management for the LEDs and programmer UC (1A, 3.3V LDO), power switch and power delivery to the ESP32-CAM;
- ESP32 programmer (*e.g.* CH340C USB to UART chip);
- USB port for optional charging, power delivery, programming, and serial communication;
- necessary electronic components for powering the 6 NIR LEDs.

The MB has been described in detail in [20]. Still, for completeness, its layout is represented in Figure 5, whereas its principal schematic as long as the components are given in the Appendix.

The system under consideration offers dual power options: a rechargeable battery or a USB cable. Nevertheless, noise from the USB cable connection may occasionally impact the achievable image quality. Furthermore, opting for battery power enhances user comfort and overall usability. We utilize the commonly used HW-357 battery charging unit, incorporating the LTC4056 constant-current/constant-voltage Li-Ion battery charger along with the STI3508 current mode step-up converter. The charging current is set at 2A, while the maximum output current at 5V stands at 1.4A. The STI3508 current mode step-up converter is part of the HW-357 battery charger module. It provides the ESP32-CAM with the necessary 5V voltage and power for other components. The ready-made HW-357 has been chosen essentially to allow others to easily reproduce the system rather than to optimize power efficiency.

Our choice of battery is the 503035 Lithium Polymer type, boasting specifications of 3.7V and 500mAh, with a maximum discharge current of 1.5A, serving as the primary power constraint for the system.

More specifically, the 500 mAh LiPo battery (503035) is connected to the HW-357 battery charger module, which is equipped with the LTC4056 constant-current/constant-voltage Li-Ion battery charger and the STI3508 current mode step-up converter. The charging current is 2 A, and the maximum output current at 5V is 1.4A. The 503035 Lithium Polymer battery (3.7 V, 500 mAh) with a maximum discharge current of 1.5 A is the system's limiting power constraint. The HW-357 battery charger module output voltage can be adjusted via a variable resistor, and the output voltage is set to 5V. The ESP32-CAM module is equipped with an AMS1117 3.3V low-voltage dropout regulator (LDO), which produces the necessary 3.3V for the ESP32S module. The STI3508 minimal input voltage is around 2V, whereas the safe LiPo battery discharge voltage level is around 2.5V to 3.0V.

D. THE 3D-PRINTED ENCLOSURE MODULES

The enclosure of the camera module is the same as the one used for the finger-vein acquisition device [20] and depicted in Figure 6.

Different fingers of the hand of the same person have different diameters, and the same finger of different hands of different persons has different diameters. Since we imagine using a ring to acquire the veins, its diameter has to be set according to the person's finger diameters. Therefore, different finger placeholders have been considered to make the acquisition fit the user's finger morphology. The user's finger diameter is first measured using some 3D-printed rings having increasing diameters in 1mm-steps, from 16 to 26 mm, and then the appropriate placeholder is used for the acquisition.

V. THE RING VEIN: THE SOFTWARE

We have implemented a comprehensive device control and data collection software using a graphical user interface (GUI). Specifically, we use an SQL backend for simple data collection and to limit human-made errors in the data collection process.

The GUI default layout can be seen in Figure 8, where both the device controls and the database controls are shown, and in Figure 9, where, together with the device controls, on the left side, the illumination controls are displayed on the right side.

Specifically, the following functionalities are displayed:

- **Device controls** – Left side from the top:
  - *Acquired image canvas* – portion of the GUI where the acquired image/video is displayed;
  - *Main controls* – controls for connecting to the device, acquiring a test image using auto illumination, streaming video;
  - *Debugging controls* – controls for debugging tasks – obtaining test image, performing *gridsearch* (obtaining a series of pictures with before set parameters, which are changed for every image) and saving images;
  - *Event log* – area where the operations with the device and database and errors are logged.
- **Database control & Camera Illuminations settings** – Right side:
  - *Database control* – controls for registering new devices and databases, enrolling new subjects, collecting and viewing collected data;
  - *Manual camera & illumination settings* – it allows the user to control illumination manually and adjust image sensor settings, *e.g.* exposure, and gain, and turn the sensor's automatic exposure on/off.

Section V-A provides more details regarding the device controls and the Automatic Illumination Module (AIM) is detailed in V-B. Section VI describes the Database Manager.

A. DEVICE CONTROLS

The device controls module is responsible for controlling every action of the device. As mentioned, the communication is made over WiFi using `GET` requests. In more detail, the device can be given the local WiFi network credentials (SSID and password). The router issues a static local IP address when connecting to the WiFi network. Afterward, the device can be accessible using this IP address. Alternatively, if no WiFi network is available, the device can serve as a WiFi host (router), and the PC can connect to the WiFi network created by the device. In this case, the IP address is present. When the device is selected, e.g., using the *Select device* drop-down menu, the device's IP address is selected, and the default image sensor parameters are uploaded.

As described in Section IV-A, the image sensor is used in manual mode, and optimal parameters are iteratively searched for by obtaining an image, analyzing it, adjusting parameters, and repeating. This functionality is described in Section V-B. Besides, the Device control module also allows performing different debugging tasks, *e.g.*, perform a *gridsearch*. In such a way, predetermined illumination/exposure and gain combinations are used, and an image is obtained for each. This functionality helps analyze these settings, obtaining a series of pictures with before-set parameters that are changed for every image.

Using the GUI, it is possible to adjust the device settings manually. For example, in our implementation of the AIM, we produce a single illumination value in the range $i \in [0, 255]$, meaning that all the LEDs are controlled jointly. However, we can adjust each LED PWM duty cycle, and thus brightness, separately, and this is one of *Manual camera & illumination settings* Tab functionalities. This helps to test the LEDs during the device manufacturing process.

B. AUTOMATIC ILLUMINATION MODULE

The OV2640 image sensor auto illumination control options are restricted, so specifying the image area used for exposure calculation is not allowed. An example of a ring vein image can be seen in the Python GUI depicted in Figure 9. Setting the correct Region of Interest (ROI) exposure in our images would be crucial. For this reason, we have chosen to pilot the image sensor in manual exposure mode and develop an automatic illumination module. Specifically, we modify the default OV2640 image sensor settings as follows:

- Turn off lens correction functionality since we aren't using the default lens the function is made for;
- Turn off the " Down-sampling, clamping and windowing" (DCW) image processing option;
- Turn off Automatic Gain Control (AGC);
- Turn off Automatic Exposure Control (AEC).
- Turn off Automatic White Balance (AWB) and AWB Gain;
- Set frame size to setting 13 – UXGA resolution – 1600×1200 pixels;
- Set the JPEG quality to the highest possible – 4.

In addition, we set three adjustable parameters as follows:

- exposure $e \in [0 \cdots 1200]$;
- illumination: currently, we use the same duty cycle for all LEDs with 8-bit PWM, so this is a single parameter $i \in [0 \cdots 255]$;
- digital gain $g \in [1, 4]$, equivalent to ISO in digital photography (a lower g would produce less noisy images.)

We adjust these parameters until we capture a vein image that meets our quality standards. Following the approach

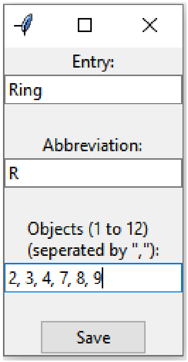

(a) *Add Device* window.

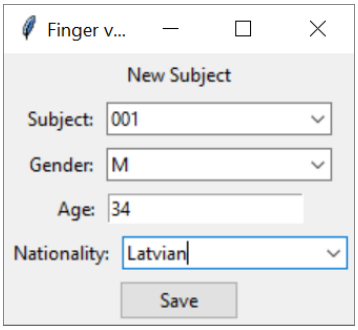

(b) *Add subject* window

FIGURE 10. **GUI: add device and add subject window.**

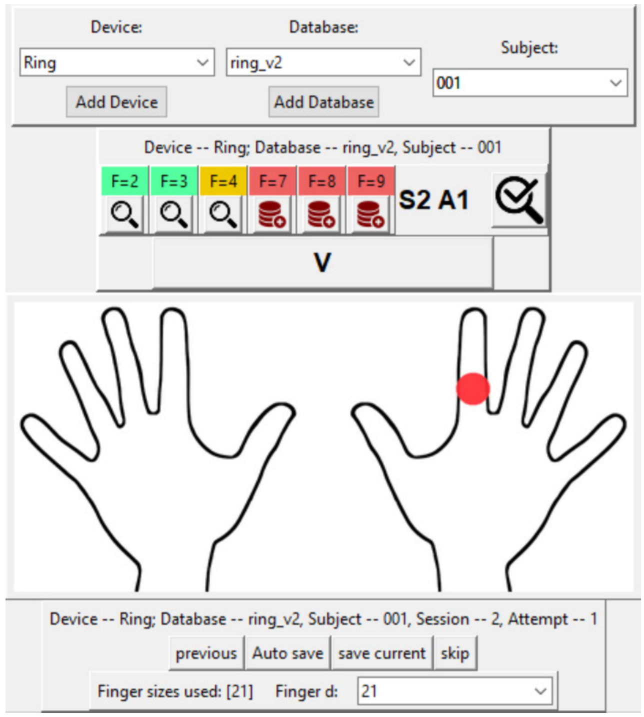

FIGURE 11. **Data collection minimized view.**

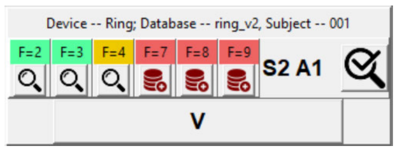

FIGURE 12. **Database view, with partially collected data.**

proposed by [23], finger vein ROI quality can be evaluated by evaluating the associated contrast, which can be computed as:

$$c = \sqrt{\frac{\sum_{i=1}^{N} (p_i - \overline{p})^2}{N}},$$

where N is the number of pixels, p_i the generic pixel i value, and $\overline{p}$ the average ROI_a pixel value calculated in the considered ROI region. We calculate c in ROI_a, a temporary square window used for illumination evaluation, represented as a green rectangle over the ring-vein image in Figure 9. Since pixel values in an 8-bit image are in the interval [0, 255], we assume that the image is over-exposed if any of the ROI_a pixel value is over 235.

VI. THE DATABASE MANAGER

Database manager uses Python SQL toolkit `sqlalchemy` and is loosely based on the *Tksqla* (Tk and SQLAlchemy) [24] example. An SQL database and a typical file-based database are used to memorize a detailed record of each of the obtained finger-vein images. The GUI is designed to work with different acquisition modalities and thus can be used with the devices we have realized in this open-source project. Data collection requires the following steps: First, the device must be selected among the possible ones. The *Add Device* dialog window can be seen in Figure 10. It is specified what type of device data is collected since, for the ring device, an extra logic is used to require the Data Operator to manually enter the finger diameter the first time each finger is used, whereas, in subsequent acquisitions, the entered value is read from the database and selected automatically. This is *triggered* by the *Abbreviation* variable. The Device entry also specifies which object, fingers, rings, or wrist will be collected by detailing the *Objects* (1 to 12) variable. The fingers are numbered from 1 to 10, from the left small finger to the right small finger. The numbers 11 and 12 stand for the left and right hand's wrist respectively, and are intended for future uses. However, the wrist device is currently under development and needs to be addressed in this paper.

In our data collection for the Ring device, we collect six finger data (both hands' Index, Middle, and Ring fingers); thus, the relevant object list is `2, 3, 4, 7, 8, 9`. The *object* approach automatically saves data for the relevant subject's finger in the data collection process. After a device entry is created, a database entry for the specific database can be added. This enables multiple databases for each device.

To register a new subject in the database, the data operator must first explain the data collection, the purpose and intended use, and other relevant details. Then, the Data Operator must ask the Subject to sign a GDPR-compliant

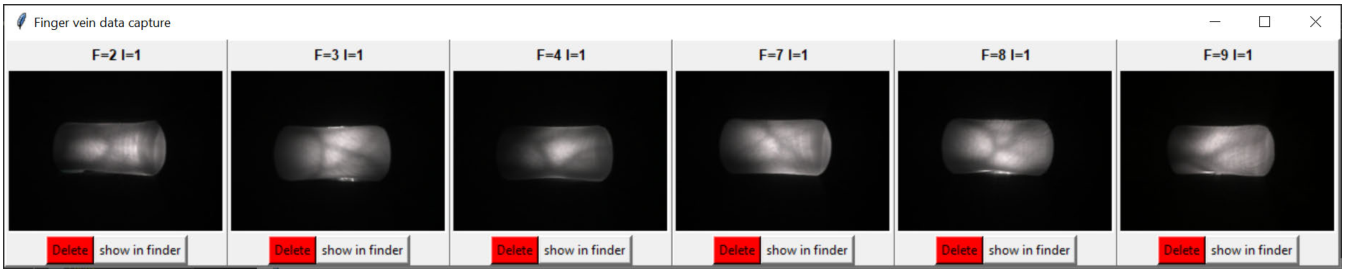

FIGURE 13. Collected data.

TABLE 2. Recognition pipeline used for 178-class Ring database, compared to the 180-subject finger vein database.

Module	Submodule	Finger vein database [20]	**Ring database**
Preprocessor	crop	Custom-made function, which converts the RGB data to monochrome and crops rectangle region from the image	Custom-made function, which converts the RGB data to monochrome and crops rectangle (273×684 pixel) region from the image
	mask	Adopted [27] ROI extractor	None used
	normalize	`HuangNormalization`	None used
	filter	`NoFilter`	None used
enhancer	–	None used	None used
extractor	–	`Maximum Curvature`; $\sigma = 8$	`Maximum Curvature`; $\sigma = 11$
algorithm	–	`MiuraMatch` $ch = 100$, $cw = 220$	`MiuraMatch` $ch = 62$, $cw = 125$

TABLE 3. Baseline `MiuraMatch/MaximumCurvature` pipeline results; ring and finger vein dataset for comparison.

	Finger, `Nom`	Finger, `Mim`	**Ring**, `Nom`	**Ring**, `Mim`
FMR	2.8% (895/32 220)	2.7% (2 590/96 660)	4.8% (1 500/31 506)	3.4% (3 186/94 518)
FNMR	2.8% (5/180)	2.6% (14/540)	4.5% (8/178)	3.4% (18/534)
HTER	2.8%	2.6%	4.6%	3.4%

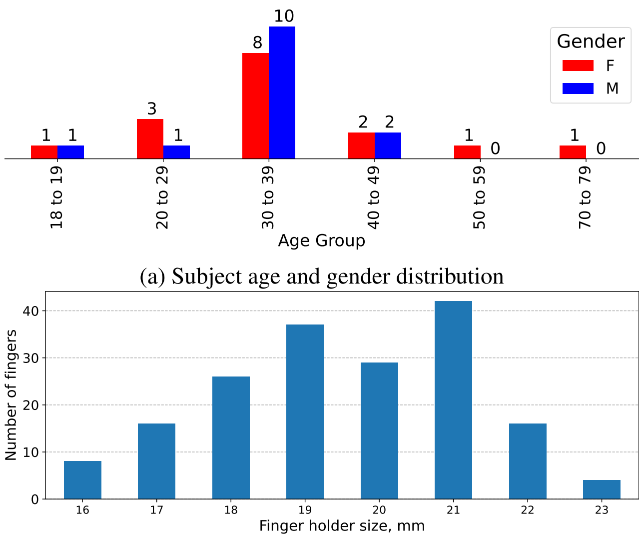

(a) Subject age and gender distribution

(b) Finger diameter statistics

FIGURE 14. Database statistics – age/gender distribution and the finger diameter statistics.

consent form. Figure 10b shows the *Add Subject* window. It consists of the following fields:

- `Subject`: Subject's designator (ID number). This number is automatically generated, starting from `001`. The subject ID number is generated by querying the database and adding `+1` to the largest ID value;
- `Gender`: gender of the subject. Currently, the possible options are: `M` – male; `F` – female; `O` – other;
- `Age`: age of the subject (in years);
- `Nationality`: nationality of the subject.

The acquisition procedure can start when the user entry is added to the database. The Data Processor selects the device, the used database, and the Subject whose data is being collected. The data collection view opens as in Figure 11. For subject/database combination, where no data have been collected, the `S1 A1` (Session 1, Attempt 1) is selected automatically. During data collection, the data processor has many tasks, such as ensuring that the subject presents the correct object, e.g., finger, inserted correctly and that AIM has correctly determined the image exposure settings. Additionally, when using the Ring device, it must be ensured that a correct-size finger adapter is used and the value is entered in the GUI. The object order is consistent with our data collection protocol. Collect all object data for the particular device in ascending order in each acquisition. After each image is obtained, the indicated finger in the guide changes to the next one. If data has been acquired for the last attempt object, it closes the current view and displays all sessions/attempts.

After each image is collected, the corresponding icon in the Database view changes color and its button functionality,

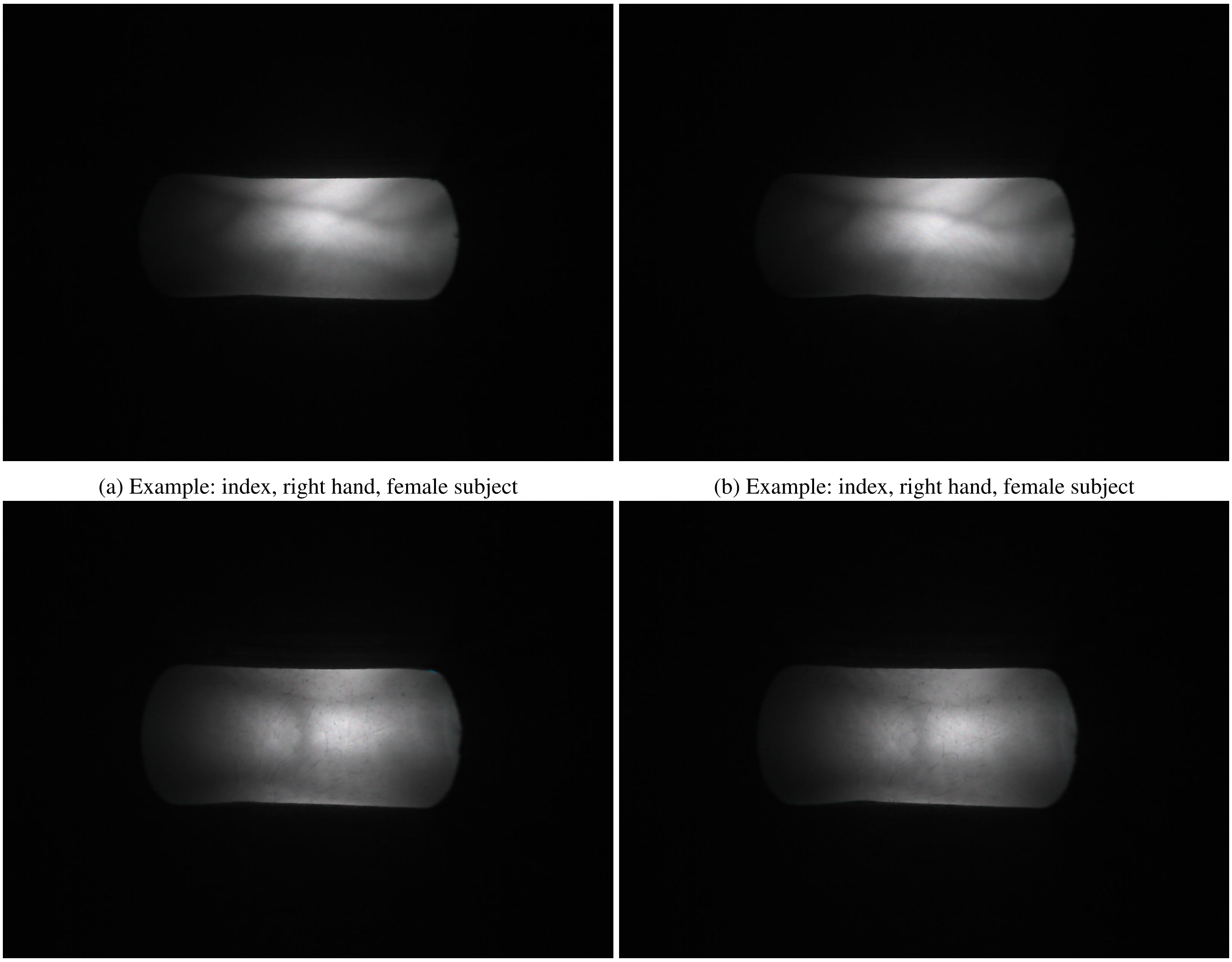

(a) Example: index, right hand, female subject
(b) Example: index, right hand, female subject
(c) Example: index, right hand, male subject
(d) Example: index, right hand, male subject

FIGURE 15. Examples of different RING images.

as in Figure 12. The collected fingers are listed as $\mathtt{F} = x$, where $x \in [2, 3, 4, 7, 8, 9]$.

VII. DATABASE

We have collected data associated to six fingers from each of the same 30 subjects considered when testing the finger vein device presented in [20]. Two of the 30 subjects couldn't remove their wedding rings, so we could not collect data from their 9th finger (right hand, ring finger), and therefore, the ring dataset consists of $30 \times 6 - 2 = 178$ class data.

The statistics of the database subjects' gender and age are shown in Figure 14a, and the finger diameter statistics are given in Figure 14b. As we can see, the finger diameter statistics resemble a Gaussian distribution with a mean value of around 19mm. Although we prepared for a more comprehensive finger size range, we have experienced fingers with 16mm to 23mm diameter.

The acquisition device renders images with a size of 1600×1200 pixels. However, the ROI interests only a limited portion of the image, depending on the different finger holders with varying sizes of openings. Therefore, the ROI is set as a portion of the image acquired using the smallest finger holder and has a 273×684 pixels area.

VIII. EXPERIMENTAL RESULTS

In this Section, we describe the processing pipeline and evaluate the device reliability and effectiveness on the collected dataset.

A. DATA PROCESSING

The recognition pipeline for the ring vein data, implemented in the Idiap's BOB [25] `bob.bio.vein` platform, [4], is summarized in Table 2, together with the pipeline used for the finger vein data analysis for comparison. We use the state-of-the-art Maximum Curvature (MC) [26] feature extractor and Miura Match (MM) comparison algorithm to directly compare results between the ring and finger vein datasets, and compare algorithm performance on other vascular databases. Besides the MC/MM pipeline, we use a simple preprocessing

TABLE 4. Main board's part list.

Name	Designator	Footprint
10μF Ceramic Capacitor 10V, 0805	C1, C6	0805
100nF Ceramic Capacitor 10V, 0603	C2, C3, C7, C8	0603
100nF Ceramic Capacitor 10V, 0805	C4, C5	0805
Switching Diode, 300mA 75V, 2-Pin SOD-323, 1N4148WS	D1, D2	SOD-323
Connector 1.27mm (0.05inch) pitch, male, 2x4 SMD	J1	2x4 SMD, 1.27mm
micro B USB 2.0 Receptacle Connector, 5pin 6.4mm	J2	micro_usb
Header 8x1 pin 2.54mm, female	J3, J4	8X1 2.54mm
battery connector (optional), 2x1 pin, 2.54mm	J5	2x1, 2.54mm
HW-357 PWR supply	PWR1	PWR_supply
NPN Transistor, 3 Pin, SOT-23, 800 mA, 32 V	Q1, Q2, Q3, Q4, Q5, Q6	SOT-23
910Ω SMD resistor, 1%, 0.1W, 0603	R1, R2, R3, R4, R5, R6	0603
10kΩ SMD resistor, 1%, 0.1W, 0603	R7, R8, R9, R10, R11, R12	0603
13Ω SMD resistor ±1%, 0.25W, 1206	R13, R14, R15, R16, R17, R18, R21	1206
0Ω SMD resistor ±1%, 1206	R19 or R20	1206
SK12D07 Toggle switch, 3Pin	SW1	SK12D07VG5
NCP1117LPST33T3G LDO, FIXED, 3.3V, 1A, SOT-223-3	U1	SOT-223
USB to UART, CH340C, SOP-16	U2	SOP-16

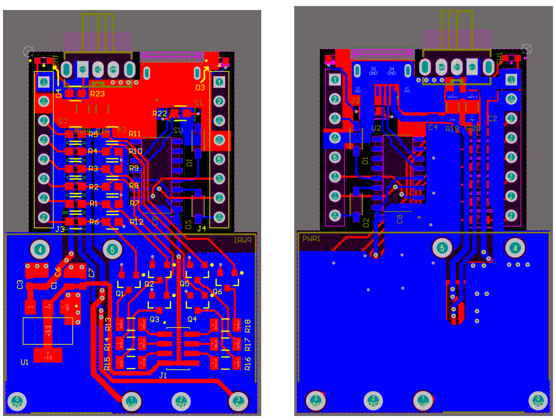

(a) (b)

FIGURE 16. Main board schematics: (a) Main board, v1.1, bottom. (b) Main board, v1.1, bottom.

that converts the obtained RGB image to grayscale and crops a 273 × 684 pixel region from each image.

B. DATA ANALYSIS

We have analyzed the ring vein data using two different protocols, namely the `nom` and `mim` protocols described hereafter:

- `Nom` (Normal operation mode) protocol uses A_1 as the enrolment (reference) sample and A_2 as a probe sample. Results are calculated in All VS All manner. Since we have $n = 178$ class data, we perform a total of $n^2 = 31\,684$ comparisons – $n = 178$ genuine scores and $n^2 - n = 31\,506$ zero-effort impostor scores.
- `Mim` (Multi-image model) protocol uses A_1 and A_2 images to construct the reference model, while A_3, A_4, and A_5 images are used as probe samples, thus utilizing the whole dataset. Fusion of the enrolment samples takes place in the scoring phase, using the mean score fusion. This means that features are extracted from all images, and each probe's features are compared against the features of both reference model images. Then, the mean score value is produced for each probe. This resembles when the user needs to provide two biometric samples in the enrolment stage. Since we use all three remaining attempt images as separate probes, there are $3 \times n = 534$ genuine comparisons and $(n - 1) \times 3 \times n = 94\,518$ zero-effort impostor scores.

Recognition results for the collected database and the two employed protocols, namely `Nom` and `Mim`, are summarized in Table 3. Using the protocol `Nom`, with a single enrollment template and a single probe for each finger, a half total error rate (HTER), i.e., the average of the computed false match rate (FMR) and false non-match rate (FNMR), at 4.6 % is obtained for ring vein images, whereas, when using the protocol `Mim`, two enroll templates, with mean score fusion, three probe images, each considered as a separate test sample, an HTER = 3.4 % is achieved.

To the best of our knowledge, in literature there is no public dataset focusing on only a small portion of the dorsal finger vein patterns, and exploited for user verification. However, for the sake of comparison, we have reported, in Table 3, the results obtained on the (palmar) finger dataset used in [20]. The results are directly comparable since the data is from the same 30 subjects using the same basic recognition pipeline. Likely, the ring device performs slightly worse than the finger one because it uses a smaller portion of the finger and, therefore, less information. A similar behavior was observed in [28] when comparing the performance achievable by exploiting only a small part of the (palmar) finger vein pattern acquired with a commercial device, with respect to the use of the whole finger. There, a performance worsening from an EER at 0.60% to an EER at 3.57% was reported when applying state-of-the-art algorithms to only 1/3 of the vein patterns available in the HKPU finger vein database, highlighting the need for developing dedicated methods for small-area vein pattern recognition.

The recognition results we here obtained are therefore excellent indicators for the viability of wearable finger vascular biometrics in the form of a ring, and testify that the dorsal side of the fingers contain vein patterns as suitable as the palmar one to perform automatic people recognition.

IX. CONCLUSION

In this paper, we have presented a novel open-source device for acquiring ring-sized dorsal finger vein data, and provided comprehensive instructions, files, and software to help other researchers replicate our setup. To test the effectiveness of our device, we conducted a preliminary data analysis using samples collected from 30 subjects. We have also made the resulting vascular image database publicly available. By employing a legacy multi-classifier/multi-matching (MC/MM) processing pipeline with a custom ROI extractor, and fine-tuning the MC σ parameter and the MM search displacement parameters, we achieved a promising HTER equal to 4.6%. Far from being exhaustive, the obtained results must be considered proof of concept about the feasibility of using the device for recognition purposes. The proposed device is a prototype that needs to be further developed and miniaturized to be employed in real-life applications, which is, however, behind the scope of this paper.

To sum up, the main advantages of the device are the following:

- it is a fully open-source data acquisition system. All components are publicly available, including schematics, a list of electronic components, 3D files for the enclosure, software for controlling the acquisition process, and software for image capture;
- it is a standalone, easily transportable device that does not require a physical connection to external peripherals;
- it has a modular design, which allows for different configurations. The acquisition and imaging modules have already been employed for finger vein acquisition, and they can also be rearranged to collect data from wrist patterns, which is currently under development and beyond the scope of this paper;
- it is low-cost, making it accessible to almost anyone interested in using it;
- it uses widely available electronic components, facilitating the manufacturing process.

The main disadvantage is its dimensions, which prevent it from being an actual wearable device as a smart ring can be. However, the purpose of this contribution is not to propose a commercially viable device but to show its feasibility in terms of quality of the collected data. With the obtained performance, using a straightforward processing pipeline, we have shown the potentiality of our device.

X. APPENDIX

In this Appendix, for the sake of completeness, the list of the main board components is listed in Table 4, and in Figure 16, the main board schematics are given.

REFERENCES

[1] J. Rice, "Apparatus for the identification of individuals," U.S. Patent 4 699 149, Oct. 13, 1987.

[2] P. K. Upputuri and M. Pramanik, "Photoacoustic imaging in the second near-infrared window: A review," *Proc. SPIE*, vol. 24, no. 4, Apr. 2019, Art. no. 040901.

[3] P. Drozdowski, B. Prommegger, G. Wimmer, R. Schraml, C. Rathgeb, A. Uhl, and C. Busch, "Demographic bias: A challenge for fingervein recognition systems?" in *Proc. 28th Eur. Signal Process. Conf. (EUSIPCO)*, Jan. 2021, pp. 825–829.

[4] IIdiap Research Institute. (2016). *Biometric Vein Recognition Library*. Accessed: Jul. 7, 2023. [Online]. Available: https://gitlab.idiap.ch/bob/bob.bio.vein

[5] R. Das, E. Piciucco, E. Maiorana, and P. Campisi, "Convolutional neural network for finger-vein-based biometric identification," *IEEE Trans. Inf. Forensics Security*, vol. 14, no. 2, pp. 360–373, Feb. 2019.

[6] D. Luo, Y. Qiao, D. Xie, S. Zhang, and W. Kang, "Palm vein recognition under unconstrained and weak-cooperative conditions," *IEEE Trans. Inf. Forensics Security*, vol. 19, pp. 4601–4614, 2024.

[7] T.-V. Nguyen, S.-J. Horng, D.-T. Vu, H. Chen, and T. Li, "LAWNet: A lightweight attention-based deep learning model for wrist vein verification in smartphones using RGB images," *IEEE Trans. Instrum. Meas.*, vol. 72, pp. 1–10, 2023.

[8] K. M. Alashik and R. Yildirim, "Human identity verification from biometric dorsal hand vein images using the DL-GAN method," *IEEE Access*, vol. 9, pp. 74194–74208, 2021.

[9] B. Huang, Y. Dai, R. Li, D. Tang, and W. Li, "Finger-vein authentication based on wide line detector and pattern normalization," in *Proc. 20th Int. Conf. Pattern Recognit.*, Aug. 2010, pp. 1269–1272.

[10] Y. Yin, L. Liu, and X. Sun, "SDUMLA-HMT: A multimodal biometric database," in *Biometric Recognition*, Z. Sun, J. Lai, X. Chen, and T. Tan, Eds., Berlin, Germany: Springer, 2011, pp. 260–268.

[11] M. Vanoni, P. Tome, L. E. Shafey, and S. Marcel, "Cross-database evaluation using an open finger vein sensor," in *Proc. IEEE Workshop Biometric Meas. Syst. Secur. Med. Appl. (BIOMS)*, Oct. 2014, pp. 30–35.

[12] B. T. Ton and R. N. J. Veldhuis, "A high quality finger vascular pattern dataset collected using a custom designed capturing device," in *Proc. Int. Conf. Biometrics (ICB)*, Jun. 2013, pp. 1–5.

[13] A. F. Sequeira, L. Chen, J. Ferryman, C. Galdi, V. Chiesa, J.-L. Dugelay, P. Maik, P. Gmitrowicz, L. Szklarski, B. Prommegger, C. Kauba, S. Kirchgasser, A. Uhl, A. Grudzie, and M. Kowalski, "PROTECT multimodal DB: Fusion evaluation on a novel multimodal biometrics dataset envisaging border control," in *Proc. Int. Conf. Biometrics Special Interest Group (BIOSIG)*. Bonn, Germany: Köllen Druck+Verlag, Sep. 2018, pp. 1–5.

[14] C. Kauba, B. Prommegger, and A. Uhl, "OpenVein—An open-source modular multipurpose finger vein scanner design," in *Handbook of Vascular Biometrics*. Cham, Switzerland: Springer, 2020, ch. 3, pp. 77–111.

[15] B. Prommegger, C. Kauba, and A. Uhl, "Different views on the finger—Score-level fusion in multi-perspective finger vein recognition," in *Handbook of Vascular Biometrics*. Cham, Switzerland: Springer, 2020, ch. 1, pp. 261–305.

[16] I. Treija. (2017). *Miniaturized Wrist Vein Scanner Biowatch Secures? 1.12 Million in Seed Funding*. Accessed: Jul. 15, 2024. [Online]. Available: https://www.eu-startups.com/2017/01/miniaturized-wrist-vein-scanner-biowatch-secures-e-1-12-million-in-seed-funding/

[17] S. S. S. R. K. Akula, S. Dasari, K. Bajaj, B. Chennoju, T. Dhandu, M. Rahman, and R. Derakhshani, "A wrist-worn diffuse optical tomography biometric system," in *Proc. Int. Conf. Biometrics Special Interest Group (BIOSIG)*, Sep. 2023, pp. 1–6.

[18] B. Hou, H. Zhang, and R. Yan, "Finger-vein biometric recognition: A review," *IEEE Trans. Instrum. Meas.*, vol. 71, pp. 1–26, 2022.

[19] A. Uhl, *State of the Art in Vascular Biometrics*. Cham, Switzerland: Springer, 2020, ch. 1, pp. 3–61.

[20] T. Eglitis, E. Maiorana, and P. Campisi, "Open-source finger vein acquisition device for biometric applications," *IEEE Trans. Instrum. Meas.*, vol. 72, pp. 1–12, 2023.

[21] Espressif Syst. (2023). *ESP32—A Feature-rich MCU With Integrated Wi-Fi and Bluetooth Connectivity for a Wide-range of Applications*. Accessed: Jul. 15, 2024. [Online]. Available: https://www.espressif.com/en/products/socs/esp32

[22] Thinker Technol. Co. (2023). *ESP32-CAM Camera Development Board*. Accessed: Jul. 15, 2024. [Online]. Available: https://docs.ai-thinker.com/en/esp32-cam

[23] H. Ma, F. P. Cui, and P. Oluwatoyin, "A non-contact finger vein image quality assessment method," in *Measurement Technology and Its Application*, vol. 239. Büch SZ, Switzerland: Trans Tech Publications, 2013, pp. 986–989.

[24] R. Jackson. (2020). *A Small App for Learning the Finer Points of Tkinter and SQLAlchemy*. Accessed: Jul. 15, 2024. [Online]. Available: https://github.com/supra621/tksqla

[25] A. Anjos, M. Günther, T. de Freitas Pereira, P. Korshunov, A. Mohammadi, and S. Marcel, "Continuously reproducing toolchains in pattern recognition and machine learning experiments," in *Proc. Int. Conf. Mach. Learn. (ICML)*, Aug. 2017, pp. 1–8.

[26] N. Miura, A. Nagasaka, and T. Miyatake, "Extraction of finger-vein patterns using maximum curvature points in image profiles," *IEICE Trans. Inf. Syst.*, vol. E90, no. 8, pp. 1185–1194, Aug. 2007.

[27] H. Lu, Y. Wang, R. Gao, C. Zhao, and Y. Li, "A novel ROI extraction method based on the characteristics of the original finger vein image," *Sensors*, vol. 21, no. 13, p. 4402, Jun. 2021.

[28] L. Yang, X. Liu, G. Yang, J. Wang, and Y. Yin, "Small-area finger vein recognition," *IEEE Trans. Inf. Forensics Security*, vol. 18, pp. 1914–1925, 2023.

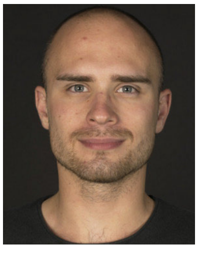

TEODORS EGLITIS (Student Member, IEEE) received the M.Sc. degree in electronics from Riga Technical University, Riga, Latvia, in 2014, and the Ph.D. degree in electrical engineering from Roma Tre University, Rome, Italy, in 2024. He was employed at the Institute of Electronics and Computer Science (IECS), initially as an Intern and later as an Electronics Engineer and a Researcher, where he also did the technical work leading to the master's thesis. In June 2016, he was at the IDIAP Research Institute, Martigny, Switzerland, on a project titled "BIOmetric Watch Activated by Veins (Biowave)" for Swiss start-up Biowatch. In 2017, he joined the School of Engineering and Digital Arts, University of Kent, as a Marie Skłodowska-Curie Early Stage Researcher, working on mobile behavioural biometrics. His research interests include signal processing, image processing, digital art, and embedded systems.

EMANUELE MAIORANA (Senior Member, IEEE) received the Ph.D. degree from Roma Tre University, Rome, Italy, in 2009, with European Doctorate Label. He is currently an Assistant Professor with the Department of Industrial, Electronic, and Mechanical Engineering, Roma Tre University. His research interests include digital signal and image processing, with a specific emphasis on biometric recognition. He was the General Chair of the Ninth IEEE International Workshop on Biometrics and Forensics (IWBF), in 2021; and the 16th IEEE International Workshop on Information Forensics and Security (WIFS), in 2024. He is an Associate Editor of IEEE Transactions on Information Forensics and Security.

PATRIZIO CAMPISI (Fellow, IEEE) received the Ph.D. degree in electrical engineering from Roma Tre University, Rome, Italy. He is currently a Full Professor with the Department of Industrial, Electronics, and Mechanical Engineering, Roma Tre University. His current research interests include biometrics and secure multimedia communications. He was a member of the IEEE Certified Biometric Program Learning System Committee. He is the Vice President for Publications for the IEEE Biometrics Council. He was the IEEE SPS Director for Student Services, from 2015 to 2017, and the Chair of the IEEE Technical Committee on Information Forensics and Security, from 2017 to 2018. He was the General Chair of the 26th European Signal Processing Conference (EUSIPCO), Italy, in 2018; the Seventh IEEE Workshop on Information Forensics and Security (WIFS), Italy, in 2015; and the 12th ACM Workshop on Multimedia and Security, Italy, in 2010. He was an Associate Editor and a Senior Associate Editor of IEEE Signal Processing Letters and an Associate Editor of IEEE Transactions on Information Forensics and Security. He was the Editor-in-Chief of IEEE Transactions on Information Forensics and Security, from 2018 to 2021.

Open Access funding provided by 'Università degli Studi Roma Tre' within the CRUI CARE Agreement